ELSEVIER

Catalysis Today 79–80 (2003) 441–451

CATALYSIS TODAY

www.elsevier.com/locate/cattod

A monolith loop reactor as an attractive alternative to slurry reactors

Thorsten Boger [a,*], Shantanu Roy [b], Achim K. Heibel [b], Oliver Borchers [c]

[a] *Corning GmbH, Abraham-Lincoln-Str. 30, D-65189 Wiesbaden, Germany*
[b] *Corning Incorporated, Corning, NY 14831, USA*
[c] *Inst. f. Chemische Verfahrenstechnik, University of Stuttgart, Stuttgart, Germany*

Abstract

A new reactor concept to replace slurry bed catalysts with monolithic catalysts is described. Different configurations are presented, all requiring minimal hardware modifications for revamp. One key feature of the new concept is that no troublesome filtration step is required, while maintaining the benefits of high catalyst effectiveness and selectivity. Furthermore, higher catalyst loads per reactor volume can be achieved with the monolith. Cold flow experiments are used to demonstrate the feasibility of the concept and to determine some empirical parameters for a simple hydrodynamic model. Characteristic performance data for the monolith reactor, such as mass transfer, heat transfer, and reactive performance, as well as their dependence on the type of monolith used are discussed on the basis of model calculations.

Keywords: Monolith; Slurry reactors; Catalysts

1. Introduction

Mechanically agitated slurry reactors and slurry bubble columns are used in many chemical and fine chemical applications. Typical examples are hydrogenations, e.g. of fatty acids and nitro-compounds, or the Fischer–Tropsch synthesis. In these reactors, small catalyst particles are used to obtain maximum catalyst utilization. Agitation by stirring or the addition of gas is used to keep the catalyst well distributed throughout the whole liquid phase. Despite the high catalyst utilization and some other claimed advantages of slurry reactors and bubble columns, the separation of the catalyst from the liquid reactants still represents a significant drawback. Attrition, which occurs as a result of the agitation, leads to a reduction in particle size and makes filtration even more difficult. In case of multipurpose units this can also lead to extended cleaning cycles to avoid contamination between different batches reducing the productivity of a given equipment. In recent years, monolithic catalysts have witnessed a growing interest for their use in multiphase systems, e.g. [1], and are used on a commercial scale for the production of hydrogen peroxide [2]. Some advantages of monoliths commonly claimed are low resistance to flow, high geometric surface area, excellent internal and external mass transfer characteristics, and mechanical integrity (no attrition). These characteristics make monoliths an attractive alternative to processes operated with slurry catalyst today since they can match the catalytic requirements and, at the same time, avoid the issues with attrition and filtration. Some recently published designs show how monoliths can replace slurry systems. One concept is the monolithic stirrer reactor

* Corresponding author.
E-mail address: borchers@icvt.uni-stuttgart.de (T. Boger).

0920-5861/03/$ – see front matter © 2003 Elsevier Science B.V. All rights reserved.
doi:10.1016/S0920-5861(03)00058-0

Nomenclature

A	area (m^2)
D	diameter (m)
F	flow rate (m^3/s)
H	height (m)
ka	overall mass transfer coefficient based on the liquid volume (s^{-1})
$k_L a$	gas to liquid mass transfer coefficient based on the liquid volume (s^{-1})
p	pressure (bar)
s	reactor aspect ratio defined as height to diameter ratio

Greek letter

ρ	density (kg/m^3)

described in [3]. In this concept, the monolithic catalyst is installed into the stirring device. Another type of concept described in [4,5] utilizes a monolithic catalyst packed into an add-on unit installed in an external loop. In both references [4,5], the gas and liquid are pumped co-currently downward though the monolithic catalyst, contained in a separate reactor vessel. A liquid re-circulation pump is used and the gas is entrained either by suction [4], or with the help of an ejector [5]. For commercially attractive retrofit options, either of these designs implies the use of the vessel used previously as the agitated slurry reactor to be used simply as a liquid storage tank as the reactant liquid is recycled through the monolith loop reactor.

In this contribution, we want to describe and discuss another alternative option of a monolith "loop reactor" in which the monolithic catalyst is installed at a fixed position *within* the existing reactor vessel promoting an internal circulation of the liquid. Advantages of this configuration are its simplicity and preclusion of any new equipment. The discussion is based on experimental results combined with theoretical analysis. The main objective is to demonstrate the technical feasibility of the concept and to present basic design criteria for such reactors.

2. Reactor concept

The general concept of such a monolith loop reactor design with internal circulation (IMLR) is shown in Fig. 1 for a number of possible configurations. Other configurations are possible as well. In all cases, the monolithic catalyst is assembled to form a fixed bed which is positioned into the reactor vessel, either concentric (Fig. 1a and b) or in an annulus along the vessel wall (Fig. 1c and d). To keep the monolithic catalyst bed in place it could be supported by legs from the bottom and side walls or it could be attached to the reactor hood. Due to the structure of the monolith, with straight channels extending throughout the whole body or bed, an IMLR resembles the configuration of a classic loop reactor with a concentric draft tube. The difference is that the individual monolith channels serve to act as a large number of such draft tubes, in a single, compact unit. As in conventional loop reactors, a liquid circulation is induced when a gas is added. Driving force for this circulation is the difference in density between the internal and external reactor space. In contrast to conventional loop reactors, the losses in driving force due to friction inside the small channels are not negligible anymore. As a result, the achieved circulation not only depends on the density differences between the riser and the downcomer but also on the type of monolith used. Examples of designs operating purely based on the

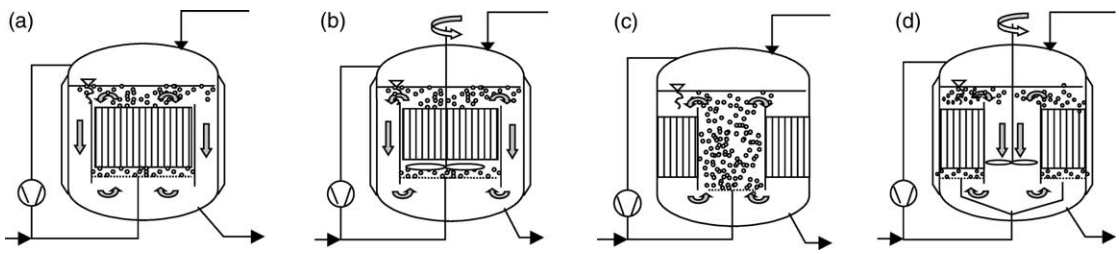

Fig. 1. Examples of possible configurations of the monolith loop reactor.

addition of a gas are shown in Fig. 1a and c. In these designs, only a simple booster compressor is required for the gas to re-circulate due to the low pressure drop which has to be overcome (typically <0.1–0.2 bar/m including the static head). Alternatively, it is possible to further enhance the driving force for the liquid circulation by means of an agitator, e.g. a propeller stirrer (see Fig. 1b and d). A similar approach was also described in [6] for a small scale catalyst testing device in which a large recycle rate was applied to minimize external mass transfer limitations in a monolithic catalyst. In case of a self-inducing stirrer this would avoid any additional equipment to supply or recycle the gas. The external heat exchange can be done as in conventional systems through the vessel wall or via extra heat exchange surfaces installed inside. Some of the key advantages of the new IMLR design in comparison to conventional slurry systems are: (i) in some cases no agitating equipment is needed (e.g. no zones with high shear forces, no moving parts); (ii) a defined flow condition and residence time distribution exists with low risk of having stagnant flow zones; (iii) the catalyst can be easily recovered without any losses due to attrition and reused, if regeneration is possible; (iv) high catalyst loading is possible without penalty on the hydrodynamics; (v) a retrofit into stirred tank and bubble column reactors is simple, requires only minimal capital spending and does not require any new plot space; (vi) low required power input to achieve a certain mass transfer compared to stirred systems; (vii) monolith channels suppress the coalescence of gas bubbles; (viii) no large scale mal-distribution of catalyst particles, or axial sedimentation of catalyst particles as often happens in slurry bubble columns.

3. Experimental

3.1. Experimental method

For the experimental work a flat bubble column setup with rectangular cross-section was used, as shown in Fig. 2 and described in more detail in [7,8]. Glass plates at the front and back end allow for the visualization and determination of the flow fields within the multiphase flow. The monoliths were placed into the column and fixed by means of a rubber mat which had sufficient grip to keep them in place as well as seal them against the glass plates. Two different widths of monolith packings were used, 300 and 400 mm, representing different ratios of the reactor to draft tube/monolith bed dimension. All other dimensions were kept as shown in Fig. 2b. Monoliths with cell densities of 25 and 100 cpsi (cells per square inch) were used, both with a void fraction of about 68–72% and hydraulic diameters of 4.2 and 2.16 mm, respectively. The monolith blocks were simply placed side by side with no sealing material in between but with about 1–2 cm gaps in axial direction. The gaps allowed for visualization and for some horizontal exchange of liquid and gas bubbles. The monolith section was separated from the empty downcomer section by a plastic bar which was slightly longer than the monolith bed and represented the wall of a draft tube surrounding the monolith bed. Since the objective was only to demonstrate the general feasibility, no measures were taken to optimize the degassing section at the top or the flow conditions at the bottom. Water was used as the liquid. Air was added to the unit through three or four of the five equally distributed sparger frits at the bottom. The gas flow rate was adjusted via mass flow controllers with a maximum total flow of 20 nl/min per sparger. The achieved gas distribution was viewed sufficiently uniform (from visual observation) for the purposes of the present study (see Fig. 2a), although it is recognized that the distribution may not optimal, especially at high liquid circulation flow rates. The analysis of the experiments was done by utilizing video equipment and measuring the local liquid velocities by Laser Doppler Anemometry (LDA) along one horizontal line in the middle of the downcomer section (at half depth of the column). In one case an additional measurement was done at the inlet into the monolith bed. Details about the equipment used can be found in [8]. The rectangular setup did not allow the use of any mechanical agitation equipment, such as the propellers discussed above (Fig. 1b and d). Therefore, the scope of the experiments was limited to studying the operation with pristine gas flow only, as shown in Fig. 1a and c.

3.2. Experimental results

In all experiments, the liquid circulation in the reactor loop was driven by the addition of a gas flow to the monolith section only. First, results for a bed

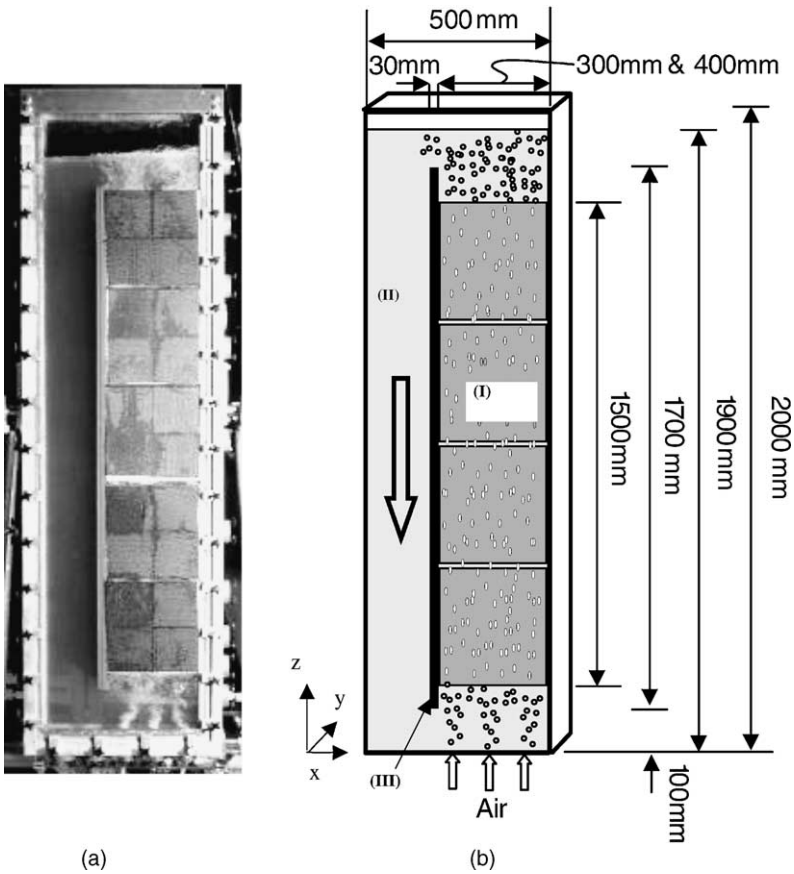

Fig. 2. Experimental setup with monoliths: (a) photo of the equipment in operation; (b) dimensions of the experimental setup with (I) monoliths, (II) downcomer section, (III) separating plastic bar, representing a draft tube. Thickness of the equipment (y-axis) was 80 mm.

of 300 mm width and 100 cpsi monoliths will be discussed. The effect of an increase in the gas feed rate on the horizontal liquid velocity profile in the downcomer is given in Fig. 3. Fig. 4 shows the relation between the superficial gas velocity and the mean liquid velocity in the downcomer for the same experiment (◇). The superficial gas velocity $u_{G0,M}$ is calculated by dividing the gas flow rate by the cross-sectional area of the monolith bed. Increasing the gas flow from 3 to 30 l/min ($u_{G0,M}$ = 0.25–2.25 cm/s) yielded a steady increase in the average downcomer liquid velocity from 6.6 to 16 cm/s. These liquid velocities correspond to liquid flow rates of 54 and 130 l/min, respectively, and demonstrate that even small gas flow rates are sufficient to initiate a significant liquid circulation. The velocity profiles are shifted towards the left wall due to the sharp 180° change in flow direction at the top of the column. A further increase in gas flow rate, e.g. to 60 l/min ($u_{G0,M}$ = 4.5 cm/s), did not yield a higher liquid flow but rather a slightly lower mean velocity of 15.4 cm/s. In addition, the observed velocity profile changed to an ideal plug flow profile. During the experiments it was observed visually that as the gas flow rate was increased more and more gas bubbles were entrained into the downcomer section (see photos in Fig. 3). This is caused by the enhanced liquid circulation and the resulting shorter residence time of the gas–liquid dispersion did not allow for a sufficient disengagement at the top of the column. Many of the larger gas bubbles (about 2–4 mm in diameter) in the downcomer section appeared to be trapped without significant vertical movement. This is caused by the

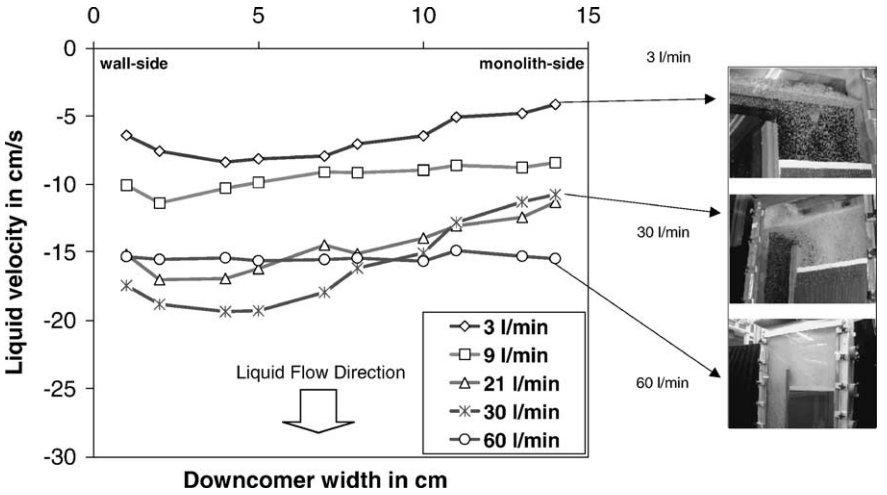

Fig. 3. Liquid velocity distribution in the middle of the downcomer at different total gas flow rates. 100 cpsi monolith, width of monolith bed 300 mm (*x*-direction). Photos show the top of the column at different flow rates.

balance between the buoyant and the gas–liquid drag forces. The measured liquid velocities are of the order of 20 cm/s, which is in line with the rise velocity typical for such bubbles. Small bubbles, having a lower rising velocity, were observed to basically follow the liquid flow path. Although the photographs in Fig. 3 deceptively suggest a very high gas hold-up in the downcomer at the gas flow rate of 60 l/min, the value estimated from the difference in liquid height during operation and after shutdown, corrected for the hold-up in the top and monolith section, was in the order of only 1–2% by volume.

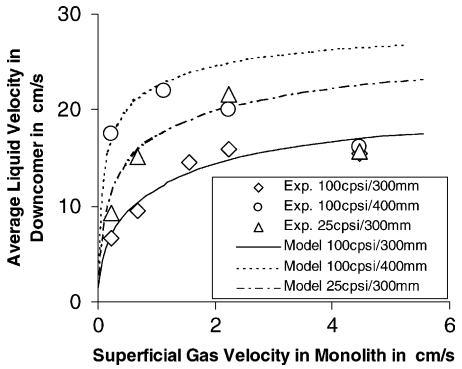

Fig. 4. Average liquid velocity in the downcomer at different total gas flow rates.

To study the effect of the ratio between the monolith bed to the downcomer area it is instructive to compare data at equal superficial gas velocity inside the monoliths. This allows for a comparison at equal frictional losses across the monolith bed. In Fig. 4, results are shown for the 100 cpsi monoliths with 400 mm bed width (○). Up to gas velocities of about 1 cm/s, significantly higher liquid velocities are achieved compared to the previous case with a 300 mm monolith bed width (◇). Correcting for the differences in the downcomer area yields similar induced liquid flow rates of 54 and 59 l/min at the lowest gas feed rates of 3 and 4 l/min for 300 and 400 mm bed width, respectively. At higher gas flow rates, however, a decrease in the achieved liquid flow is observed converging to almost identical liquid velocities at 4.5 cm/s superficial gas velocity.

Increasing the size of the monolith channels reduces their resistance to flow. The impact of this is shown in Fig. 4 for 25 cpsi monoliths with a bed width of 300 mm (Δ). Up to gas velocities of 2.25 cm/s about 35–60% higher liquid flow rates were achieved compared to the 100 cpsi monoliths at identical bed width and gas flow rates. Further increasing the gas flow rate again resulted in a drop in liquid circulation and the same value as for the 100 cpsi experiments with 300 and 400 mm bed width was obtained. In the left part of Fig. 5, the velocity profiles in the downcomer are shown for this experiment. The measured peak

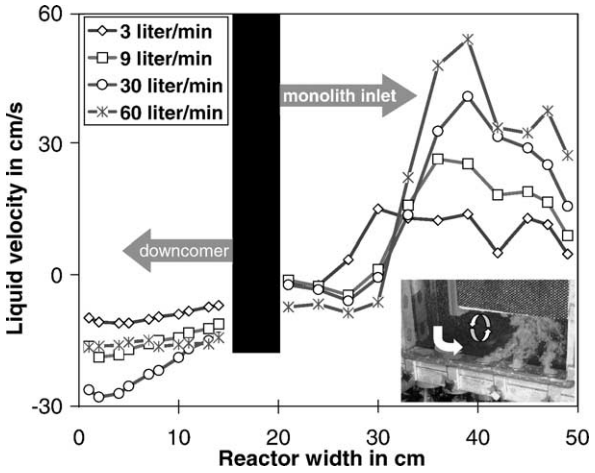

Fig. 5. Liquid velocity distribution in the downcomer and the inlet into the monolith bed at different total gas flow rates. 25 cpsi monolith, width of monolith bed 300 mm (*x*-direction). Photo taken at 60 l/min.

velocities approached almost 30 cm/s and the observed velocity profiles are qualitatively comparable to those shown in Fig. 3 for 100 cpsi, again with the shift to ideal plug flow at the high gas flow rate of 60 l/min.

In the experiments with the high liquid circulation it was observed that the circulating water resulted in a flow with a strong horizontal velocity component at the inlet to the bottom section, because of which only a part of the monolith was properly supplied with gas (see photograph in Fig. 5). To quantify this effect the velocity profile was measured below the monolith for the most severe case with 25 cpsi monoliths. Results are shown in Fig. 5. Except for the experiment at 3 l/min all cases show a change in flow orientation at about 2/3 of the bed width. The flow close to the separating bar (draft tube) was directed downwards indicating that some of the liquid was circulating either just below the monolith or throughout the whole monolith bed (note, that the integral upward and downward flow in the measurement plane were essentially the same as expected from the conservation of mass). The video imaging of the bottom section suggested that the circulation was mainly limited to the area below the monolith bed and it appeared from the movement of the bubbles that there was a strong horizontal movement just below the monolith bed. Indeed, visual observations at the gaps between the monolith blocks and the top of the monolith bed indicated that gas bubbles were rising through almost the entire cross-section.

4. Hydrodynamic model of the reactor

To gain a better understanding of the observed phenomena and to facilitate the reactor design a simple hydrodynamic model was developed. Such a model is based on a force balance requiring that the difference in pressure between the bottom of the reactor, p_b, and the liquid surface at the top, p_t, is the same throughout the whole cross-section. This is shown schematically in Fig. 6, in which the reactor is split into two zones: the downcomer section, marked by a '*D*', on one side and the monolith riser section on the other side (marked with a '*M*'). The bottom turn 'U_B', an optional agitation device '*P*', the head section '*H*' and the top turn 'U_T' are all important elements that contribute to the fluid pressure drop. For steady state operation, it is required that the following Eq. (1) holds:

$$\Delta p_D = \Delta p_{U_B} + \Delta p_P + \Delta p_M + \Delta p_H + \Delta p_{U_T} = p_t - p_b \quad (1)$$

In this equation, the subscripts refer to the contribution of the various sections described above. Each of these terms can be calculated by well known correlations. A generalized form can be written as

$$\Delta p_x = \rho_{\mathrm{eff},x} \left\{ H_x g - H_x \frac{\zeta_x}{2} \left(\frac{F_x}{A_x} \right)^2 \right\} \quad (2)$$

with the subscript *x* representing the various characteristic values to be used in each section. In all sections, the effective density was calculated by considering the local gas hold-up. For the turns, U_B and U_T, only the frictional losses were considered with a friction factor of $z = 0.98$ for a 90° kink [9]. The velocities were calculated with the free area for horizontal flow. In the bottom and head section, '*P*' and '*H*', no frictional losses were considered and the effect of an agitating device was considered by adding a certain Δp_{agit}. The calculation of the pressure drop across the monolith section was done with literature correlations as for example given in [4,5]. In the downcomer section, initially only the frictional losses of the reactor wall and

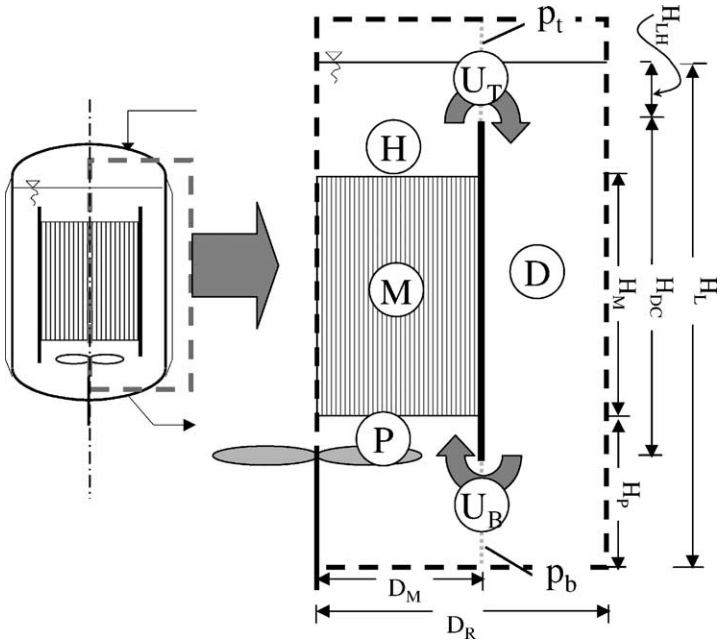

Fig. 6. Schematic of the different zones considered in the hydrodynamic model.

draft tube wall were considered, e.g. as described in [9] for tubes or an annulus. However, these calculations yielded significantly higher liquid velocities at higher superficial gas velocities as compared to the experiments, especially in the cases with 25 cpsi monoliths or the slimmer downcomer. The reduced density in the downcomer due to entrained gas bubbles was found to be not sufficient to explain the differences since an unrealistic high gas hold-up in excess of 40% would have been required. Introducing an additional term which considers frictional losses due to the flow around stagnant (or rising) gas bubbles in the downcomer, as observed in the experiments, was found to yield good results. The mathematical approach taken was based on the assumption that the bubbles can be treated as spherical particles in a fixed bed and the well known Ergun equation was used without modification. The only remaining unknown was the liquid hold-up in the downcomer. A simple two-parameter correlation was fitted empirically to best describe the experimental observations. The results from this hold-up correlation are in fair agreement with the estimations obtained from the change in liquid level during operation and shut down. Results obtained with this simple hydrodynamic model are shown in Fig. 4. A very good agreement is obtained for the 100 and 25 cpsi monolith with a bed width of 300 mm. The strong drop in liquid circulation as observed especially for the 100 cpsi monolith with a bed width of 400 mm and the 25 cpsi monolith at the highest gas flow could not be predicted. However, the deviations observed are expected to be mainly due to the maldistribution at the monolith inlet and some shortcomings of the simple hold-up model for the downcomer. Since these effects would be eliminated in a commercial reactor no further measure was taken to improve the model.

5. Discussion

The basic feasibility of the proposed reactor concept has been demonstrated in Section 3. Potential areas for improvement for a possible commercial reactor design are for example, to have an effective disengagement zone and to have a gas distribution system that is not affected by the re-circulating liquid. Such designs are already available or can be adapted from the work done on conventional loop reactors, e.g. [10].

In this section, we present a design concept for what we envision as a typical commercial monolith loop reactor. The design is evolved by combining the hydrodynamic model presented earlier, with standard correlations for the mass and heat transfer in three-phase monoliths. The gas to liquid mass transfer is described as $k_L a$ based on the total liquid volume and was determined with contributions from the monolith section [4,5,11,15] as well as the top and downcomer section [10]. The overall mass transfer from gas to the solid catalyst surface was determined by assuming a resistance in series model. The heat transfer between the liquid and a heating jacket at the cylindrical section of the reactor shell was determined by the correlation given in [9] and is expressed as specific heat removal rate, Q_W, per liquid volume. For the discussion, a reactor with the dimensions as described in Table 1 is considered. In addition to the monolith structures included in the experimental study presented above, a 400 cpsi monolith is also considered as a possible design option. This monolith structure has a hydraulic diameter of 1 mm and a similar void fraction as the others of about 70%. The general feasibility to operate monoliths which such a high cell density and small channels in co-current gas/liquid upflow was demonstrated previously, e.g. [16–18].

Table 1
Parameters of the reactor and monolith bed used in the discussion

Parameter	Base value	Range studied
Reactor		
Diameter, D_R	2.5 m	–
Height, H_L	5 m	–
Slenderness, s	2	1–20 (at constant volume and monolith to vessel ratios)
Monolith bed		
Diameter, D_M	2 m	1.25–2.35 m
Height, H_M	3 m	–
Distance from bottom, H_p	0.8 m	–
Draft tube		
Height, H_D	4 m	–
Distance from liquid level, H_{LH}	0.5 m	–
Gas feed flow	1000 N m^3/h	20–10000 N m^3/h
Liquid feed flow	0 m^3/h	–
Specific agitation, P/V_L	0 W/m^3	0–5000 W/m^3
Monolith structure	25, 100, 400 cpsi	–
Liquid/gas	Water/air at 20 °C, 1 bar	–

5.1. Effect of the feed gas flow

In Fig. 7a, results are shown for the achieved liquid circulation and the gas hold-up in the downcomer as calculated by the model and a reactor with the base dimensions from Table 1. Initially, the induced liquid circulation rate follows the increase in the gas feed rate until it reaches a maximum. In this region the gravity driven forces dominate and the liquid flow is driven by the steady increase in gas hold-up inside the monolith resulting in a larger density difference between the monolith riser and the downcomer section. Beyond the maximum a further increase in the gas feed rate has the opposite effect. In this region, the frictional losses inside the monolith, being a strong function of the gas velocity, are dominating and cannot be balanced by a further increase in the density difference. The lower liquid flow rates for monoliths with higher cell density are caused by their higher resistance to flow. This also results in a shift in the maximum to lower gas velocities since the region in which the frictional losses determine the operation begins earlier. In general, the achieved circulation rates of 500–1500 m^3/h are quite significant considering the reactor volume of 24.5 m^3.

In Fig. 7b, results are shown for the total mass transfer per total liquid volume inside the reactor (oxygen in water). The local mass transfer rates inside the monolith are higher. The gas to liquid mass transfer, $k_L a$, increases almost proportional to the gas flow. Notably, there is almost no difference between the different types of monolith (channel size) as the model is based on experimental data which show the same behavior [15]. For reference purposes, we also estimated the gas to liquid mass transfer coefficients achieved in a conventional bubble column or stirred tank of the same reactor geometry (see Table 1). The correlations given in [12] were used. For the comparison the gas flow was set to 1000 N m^3/h, corresponding to a superficial velocity of about 0.1 m/s in the monolith. The power input via the stirrer was set to 400 W/m^3_L, a reasonable value that allows for a comparison at roughly identical specific power input for all three reactor types.

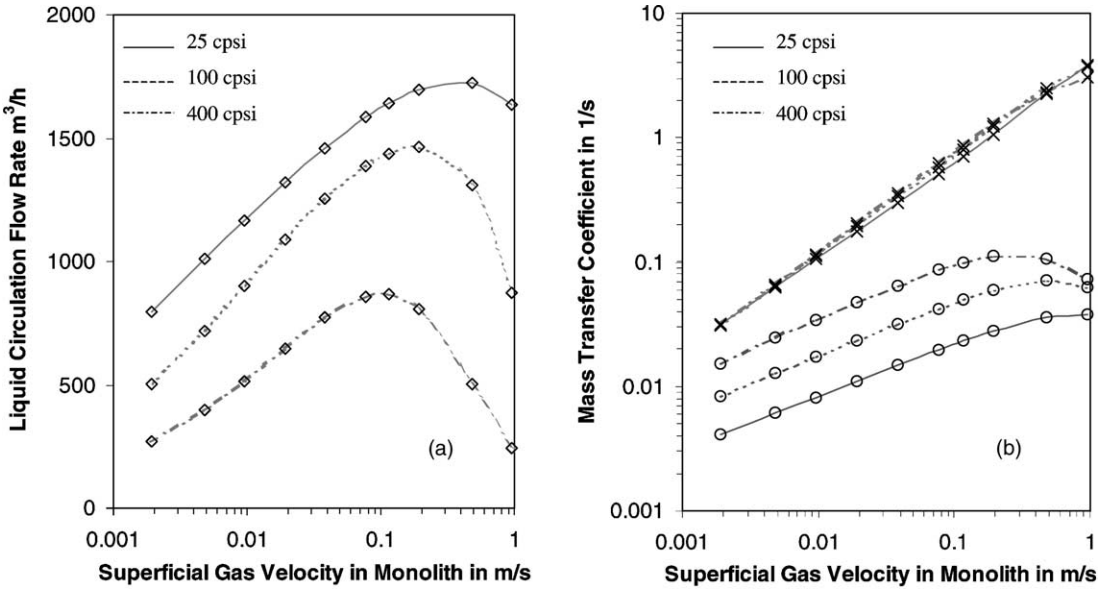

Fig. 7. Effect of gas feed flow rate on (a) the liquid circulation (◇) and (b) the gas to liquid (*x*) and the overall gas to solid (○) mass transfer for oxygen in water. Modeling results with conditions and dimensions as base case in Table 1.

The negative impact of solid particles on $k_L a$ in bubble columns and stirred tanks [13] was not considered to obtain conservative results. The calculated values for $k_L a$ were 0.58, 0.017 and 0.11 s^{-1} for the monolith, the bubble columns and the stirred tank, respectively. This shows the superior gas–liquid contacting performance of the monoliths.

The overall mass transfer *ka* also increases with the gas flow rate and goes through a maximum at high gas flows. The eventual drop in the value of this quantity is the indirect result of the change in liquid flow at extremely high gas flow rate. Fig. 7b also shows that the overall mass transfer coefficient, *ka*, is a strong function of the monolith cell density and correlates roughly to the geometric surface area. In the example reactor, the installed solid surface area per total liquid is 1040 m^2/m^3 for the 400 cpsi monolith. This value can be easily increased by changing the monolith to liquid volume ratio (or by using an even higher cell density monolith). Obviously, there are practical limits to increasing the geometric surface area and the typical practical limit is expected to be of the order of 1500 m^2/m^3. For comparison, a slurry reactor filled with 100 μm particles and a solid volume fraction of 3% yields a specific surface area of 1800 m^2/m^3. The resulting overall mass transfer coefficient *ka* is estimated to be in the order of 0.08 s^{-1}, compared to the 0.07 s^{-1} for the monolith. This shows that the favorable hydrodynamic conditions inside the monolith channels can at least partially recover disadvantages in specific solid surface area.

We have also estimated the heat removal capabilities of the system discussed above. In this arrangement and a gas feed rate of 1000 N m^3/h the liquid volume based reactor heat transfer coefficients were estimated to be in the range of 1–2 kW/(m_L^3 K), which is quite in the order of a stirred reactor of this geometry and exchange area, when an overall heat transfer coefficient of 300 W/(m^2 K) is assumed [14].

5.2. Effect of the reactor aspect ratio H_L/D_R

The effect of the reactor aspect ratio on the liquid circulation and the external heat removal efficiency at constant volumes of the reactor and the monolith is shown in Fig. 8. As the reactor becomes slimmer the induced liquid circulation drops. This is caused mainly by the change in monolith bed area resulting from an increase in the height to diameter area (at constant volume). Since the gas velocity inside the monolith

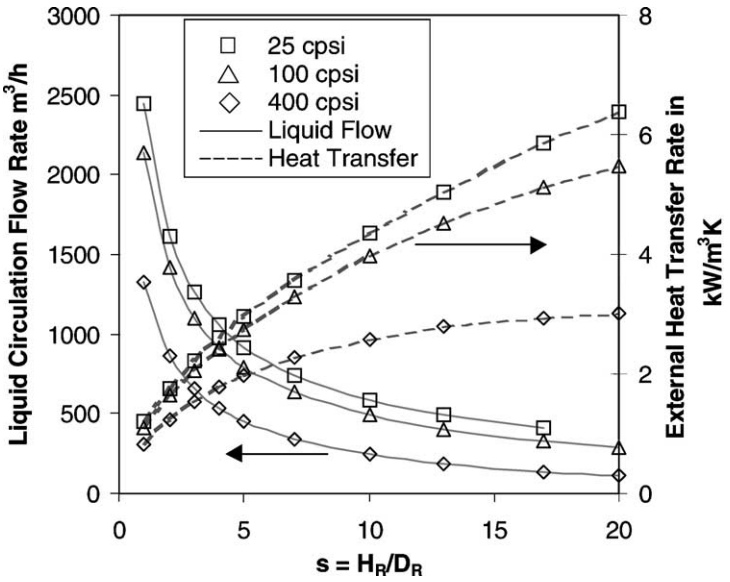

Fig. 8. Modeling results showing the effect of the reactor aspect ratio on the liquid circulation and the external heat transfer efficiency at a gas flow of 1000 N m^3/h and the base data from Table 1.

is inverse proportional to the monolith bed area and the monolith length this goes along with higher frictional losses across the monolith and a reduction in the induced liquid flow. With respect to the external heat transfer efficiency of the reactor the aspect ratio or slenderness is a very powerful parameter for the design. The calculated liquid volume based heat transfer coefficient increases steadily with the reactor slenderness. The mass transfer characteristics, $k_L a$ and ka, of the monolith reactor are found to be only slightly effected by the reactor slenderness (not shown).

5.3. Other parameters

We also investigated the influence of a number of other characteristic parameters. A detailed discussion is beyond the scope of this paper. Therefore, only a few more comments are made. The effect of a liquid feed and withdrawal flow, as it would occur in a continuous operation, was found to be negligible since the typical feed rates are much smaller than the circulating flow rates. The use of mechanical agitation to increase the liquid circulation rate is effective beyond a specific power input of ca. 100 W/m^3. The gained improvements are limited with respect to the mass transfer but can be significant for the external heat transfer. Variation of the monolith bed to reactor diameter ratio, D_M/D_R, showed an optimum with respect to the liquid circulation rate. This optimum depends on the monolith structure and values of about 0.66, 0.77 and 0.84 were found for the 25, 100 and 400 cpsi monolith beds, respectively. A slight increase in the liquid volume based mass transfer coefficients, ka and $k_L a$, and a significant increase in the external heat transfer efficiency were found as higher ratios for D_M/D_R were used.

6. Conclusions

The general feasibility of the proposed monolith reactor design with internal recycle was demonstrated by experiments on an industrially relevant scale. The gas supply section, as well as the degassing section was identified as important areas for improvement. The well-defined geometry of the system allows to sufficiently capture the hydrodynamic features with a relatively simple mathematical model. The combination with literature data for mass and heat transfer enabled us to estimate some of the key characteristics

of a commercial scale reactor. A superior gas to liquid $k_L a$ factor and similar overall mass transfer performance was found compared to conventional slurry reactor systems. This combined with the various benefits like the possibility to fully recover the catalyst, the avoidance of any tedious filtration steps, the flexibility in design, the simplicity and the minimal required investment support the conclusion that the proposed monolith loop reactor design can be a very attractive replacement option for applications where slurry catalyst is used today.

Acknowledgements

The authors would like to thank Bastiaan Nijland, who worked at Corning GmbH as an intern and performed the experiments at the University of Stuttgart as well as helped with the analysis of the data.

References

[1] F. Kapteijn, T.A. Nijhuis, J.J. Heiszwolf, J.A. Moulijn, Catal. Today 66 (2001) 133–144.
[2] R.E. Edvinsson Albers, M. Nyström, M. Silverström, A. Sellin, A.-C. Dellve, U. Andersson, W. Herrmann, T. Berglin, Catal. Today 69 (2001) 247–252.
[3] R.K. Edvinsson Albers, M.J.J. Houterman, T. Vergunst, E. Grolman, J.A. Moulijn, AIChE J. 44 (1998) 2459–2464.
[4] J.J. Heiszwolf, L.B. Engelvaart, M.G. van den Eijnden, M.T. Kreutzer, F. Kapteijn, J.A. Moulijn, Chem. Eng. Sci. 56 (2001) 805–812.
[5] R.R. Broekhuis, R.M. Machado, A.F. Nordquist, Catal. Today 69 (2001) 87–93.
[6] A.C.J.M. van de Riet, H. Vonk, X. Xu, E. Otten, A. Cybulski, A. Stankiewicz, R.K. Edvinsson, J.A. Moulijn, React. Kinet. Catal. Lett. 60 (2) (1997) 339–349.
[7] S. Becker, A. Sokolochin, G. Eigenberger, Chem. Eng. Sci. 49 (1994) 5747–5762.
[8] O. Borchers, C. Busch, A. Sokolochin, G. Eigenberger, Chem. Eng. Sci. 54 (1999) 5927–5935.
[9] L.P.B.M. Janssen, M.M.C.G. Warmoeskerken, Transport Phenomena Data Companion, Delftse Universitaire Pers.-III, ISBN 90-407-1302-2.
[10] H. Blenke, Loop reactors, in: T.K. Ghose, A. Fiechter, N. Blakebrough (Eds.), Advances in Biochemical Engineering, vol. 13, Springer-Verlag, Berlin, 1979, pp. 122–214.
[11] M.T. Kreutzer, J.J. Heiszwolf, T.A. Nijhuis, F. Kapteijn, J.A. Moulijn, in: Proceedings of the Poster at Annual Conference of Dutch Chemical Engineers in Lunteren, NL, January 2000.
[12] E.S. Gaddis, Chem. Eng. Proc. 38 (1999) 503–510.
[13] A.A.C.M. Beenackers, in: G. Ertl, H. Knözinger, J. Weitkamp (Eds.), Handbook of Heterogeneous Catalysis, vol. 2, VCH, 1997, pp. 1444–1464.
[14] VDI Wärmeatlas, eighth ed., 1997, Section Cc 1.
[15] M.T. Kreutzer, P. Du, J.J. Heiszwolf, F. Kapteijn, J.A. Moulijn, Chem. Eng. Sci. 56 (2001) 6015–6023.
[16] L.L. Crynes, R.L. Cerro, M.A. Abraham, AIChE J. 41 (1995) 337–345.
[17] A.A. Klinghoffer, R.L. Cerro, M.A. Abraham, Ind. Eng. Chem. Res. 37 (1998) 1203–1210.
[18] G. Bercic, A. Pintar, Chem. Eng. Sci. 52 (1997) 3709–3719.